Journal of Non-Crystalline Solids 624 (2024) 122731

Contents lists available at ScienceDirect

Journal of Non-Crystalline Solids

journal homepage: www.elsevier.com/locate/jnoncrysol

Application of topological constraint theory to alkali borate and silicate glass systems

N. Keninger, S. Feller *

Physics Department, Coe College, Cedar Rapids, IA 52402, USA

ARTICLE INFO

Keywords:
Topological constraint theory
Glass transition temperature
Fragility
Glass structure
Borate
Silicate

ABSTRACT

Principles of Topological Constraint Theory (TCT) were applied to alkali borate and silicate glass systems using intermediate range structural models over wide compositional ranges. The structural model for lithium borate was derived from the Feller, Dell, and Bray model [1] and extended to the terminal composition at $R = 3$ where R is the molar ratio of lithium oxide to borate. The sodium borate structural model was built using both NMR [2] and Raman [3] data, and also included carbonate retention in the glass [4]. This model was extended to $R = 3$ similarly to the lithium borate system. The silicate system models were created from ^{29}Si NMR data [5] and also incorporated carbonate retention where necessary [6].

Constraint models considered the effect of intermediate range structures on the system, and also incorporated the effect of "loose" alkali which is not directly associated with a non-bridging oxygen. Constraint models of the alkali borate, silicate, and borosilicate systems were then used to predict properties such as glass transition temperature and fragility.

1. Introduction

Topological Constraint Theory (TCT) was first introduced by Phillips & Thorpe in 1985 [7], where it found its initial success in predicting the properties of chalcogenide glasses, though we find that it is successful in predicting the properties of oxide glasses as well. The foundation of TCT is the constraints, which are defined for this purpose as ways in which an atom's degrees of freedom are limited. By gaining an understanding of the structure and finding the ways in which constraints change over a compositional range, we can predict properties of the glass by relating the change in constraints, or inversely the change in the degrees of freedom, to properties such as glass transition temperature, fragility, and elastic modulus. This method poses some advantages, one of which being that only one reference point is needed to fit the model to the data throughout its entire compositional range, assuming the structure and constraints are known. An unavoidable consequence of constraint theory however stems from the structural knowledge that constraints are based upon. If the structure is not well known or deviates from the accepted structure, it can percolate to changes in how TCT would otherwise predict the constraints and properties. This work is a broad extension of the work on lithium borates done by Takeda et al. [8].

2. Borate structure

One of the primary challenges of constraint theory comes from the need for an accurate structural model to base constraints upon for each individual glass system. Thanks to insights on the nature of constraints in certain borate rings from Takeda et al. [8], it was decided that an intermediate-range structural model would be necessary for the borate glass systems.

For the lithium borate system, the structural model was derived from the previously existing Feller, Dell, and Bray model [1]. The borate network is divided up into a series of ring structures, where the structural model describes the fraction of each unit present at a given composition. The units are as follows: Boroxol (B^3); Tetraborate, which is a Pentaborate ring connected to a Triborate ring (T^3, T^4); Diborate (D^3, D^4); Metaborate (M^3); Pyroborate (P^3); Orthoborate (O^3); Loose 4-coordinated Boron (L^4). These are then subdivided into three and four coordinated borons corresponding to each unit, portrayed by the superscript on each unit label. Lewis diagrams of each ring structure are portrayed in Fig. 1 [1]. The overall glass structure shown as fractions of borate units is shown in Fig. 2 [1]. From these fractions the structure can be simplified into a set of network forming species that each have their own unique constraints. These network forming species for the borate

* Corresponding author.
E-mail address: sfeller@coe.edu (S. Feller).

https://doi.org/10.1016/j.jnoncrysol.2023.122731
Received 28 September 2023; Received in revised form 8 November 2023; Accepted 11 November 2023
Available online 16 November 2023

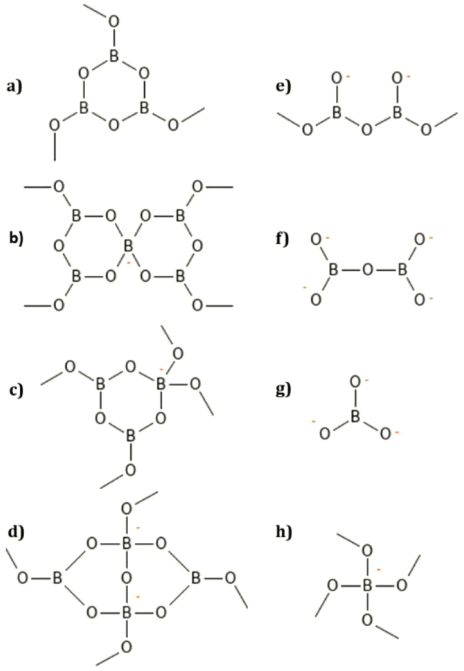

Fig. 1. Structural diagrams of borate rings [1]. (a) Boroxol; (b) Pentaborate; (c) Triborate; (d) Diborate; (e) Metaborate; (f) Pyroborate; (g) Orthoborate; (h) Loose N4.

glass systems are classified as follows: standard 4-coordinated borons (B^{4*}); 4-coordinated borons that exist in a diborate ring (D^{4*}); standard 3-coordinated borons (B^{3*}); bridging oxygens (O^{B}); cluster forming modifier ions attached to non-bridging oxygens (M^{NB}, where M is the modifier ion, such as Na^{+} or Li^{+}); 'Loose' modifier ions which are not directly associated with a non-bridging oxygen (M^{L}). 4-coordinated borons in diborate rings are classified separately because as shown by Takeda et al. [8]. A redundant angular constraint is counted on one of the 4-coordinated borons in the diborate ring when only considering short range order. Evolution of the fractions of each network forming species throughout the lithium borate glass composition are shown in Fig. 3.

For the sodium borate system, a structural model was built using NMR data from Jellison and Bray [2] alongside Raman spectroscopy data from Kamitsos and Karakassides [3]. The NMR data was used to provide a fraction of 4-coordinated borons (N^{4}) throughout the compositional range while the Raman data was used to determine which intermediate range structural units were present in each compositional region in the glass. Stoichiometric conservation principles were then used to derive the full structural model seen in Fig. 4. It should be noted that unlike the lithium borate system, the sodium borate system has some added complexity in the form of two new borate ring structures, ditriborate (Dt^{3}, Dt^{4}) and dipentaborate (Dp^{3}, Dp^{4}), which are structurally similar to their counterpart triborate and pentaborate rings but with an extra 4-coordinated boron, and carbon retention in the form of CO_3^{2-}. The amount of carbonate retained in the glass was modeled as linear after insights by Kasper et al. [4]. In calculating the fraction of network forming species, CO_3^{2-} ions were taken to have no impactful β-constraints and have one associated M^{NB}. As with the lithium borate system, this was then broken down into the series of network forming species to be used in considering constraints, as shown in Fig. 5.

3. Silicate structure

The structure for the alkali silicate glass systems can be described using simpler short range ordered units since unlike in the borate network, there are no known silicate structures that would cause redundant counting of constraints. This means that we can describe units in the silicate network by simply looking at the number of bridging oxygens that exist in a silicon tetrahedra, otherwise known as Q^{n} units, where *n* is the number of bridging oxygens attached to the silicon atom. In lithium silicate, only these Q^{n} units exist in the glass, and can range from Q^{4} units, which have only bridging oxygens, to Q^{0} units, which are completely saturated with non-bridging oxygens. The lithium silicate structural model shown in Fig. 6 was derived from NMR data from Maekawa et al. [5] and Larson et al. [9]. This was then used to derive the network forming species fractions shown in Fig. 7, like how was done for the borate systems. In this system the network forming species simply consist of each of the Q units as well as the corresponding bridging oxygens and alkali ions.

Sodium silicate behaves very similarly to lithium silicate in terms of its structure, but like the sodium borate system, retains carbon in the form of carbonate [6]. Not only does this add another unit, but because the carbonate ion requires two accompanying sodium ions that would otherwise be incorporated into the silicate network, the glass forming range is extended from $R = 2$ to approximately $R = 3$. The sodium silicate structural model shown in Fig. 8 was derived from NMR data from Maekawa et al. [5] and Barrow et al. [6]. This was then used to derive the network forming species fractions shown in Fig. 9.

4. Constraints

When identifying the constraints that exist in an oxide glass structure, there are 4 primary types of constraints that have typically been

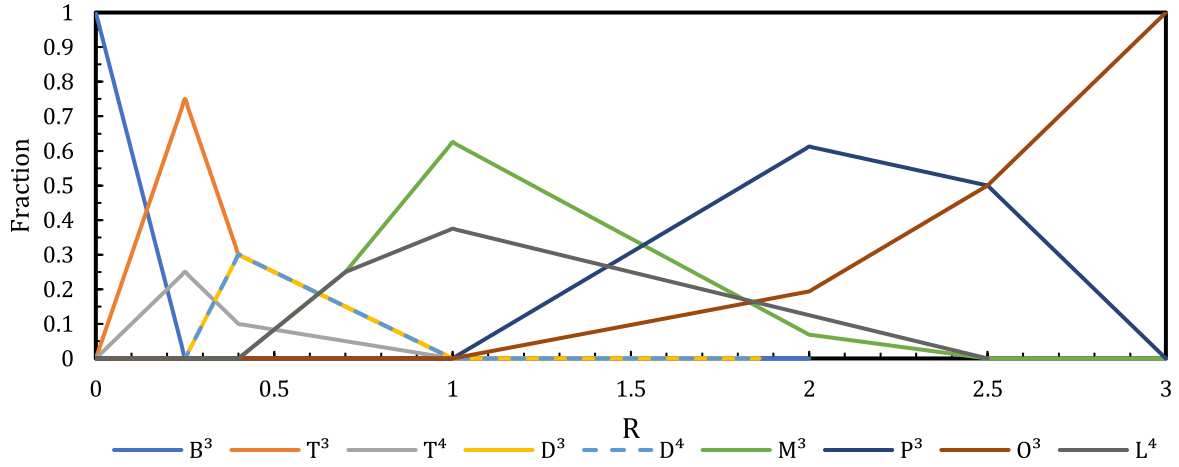

Fig. 2. Intermediate Range Structural Model of Lithium Borate Glass ($RLi_2O * B_2O_3$).

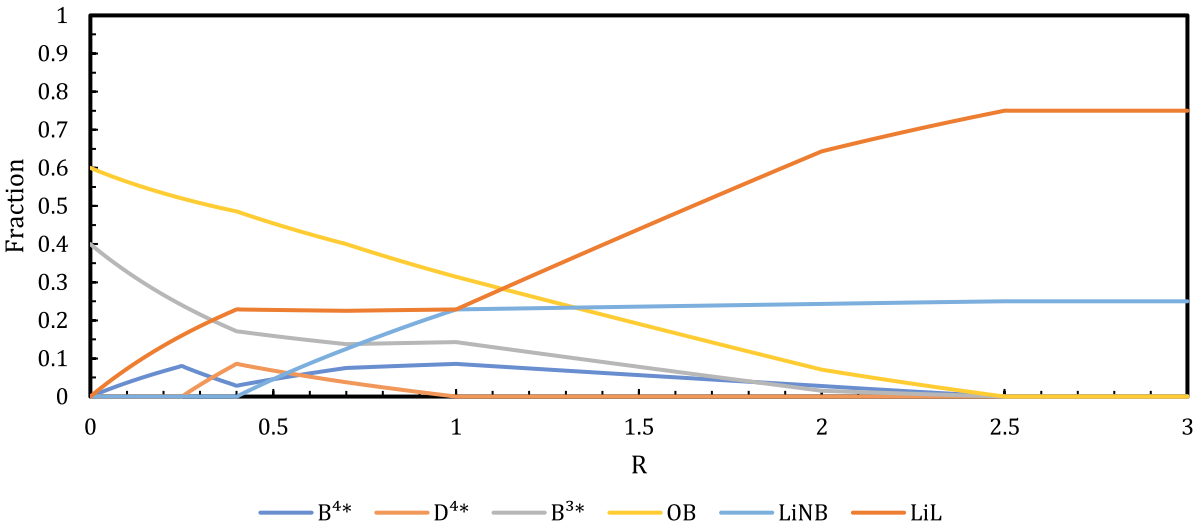

Fig. 3. Fraction of Network Forming Species in Lithium Borate Glass ($RLi_2O * B_2O_3$).

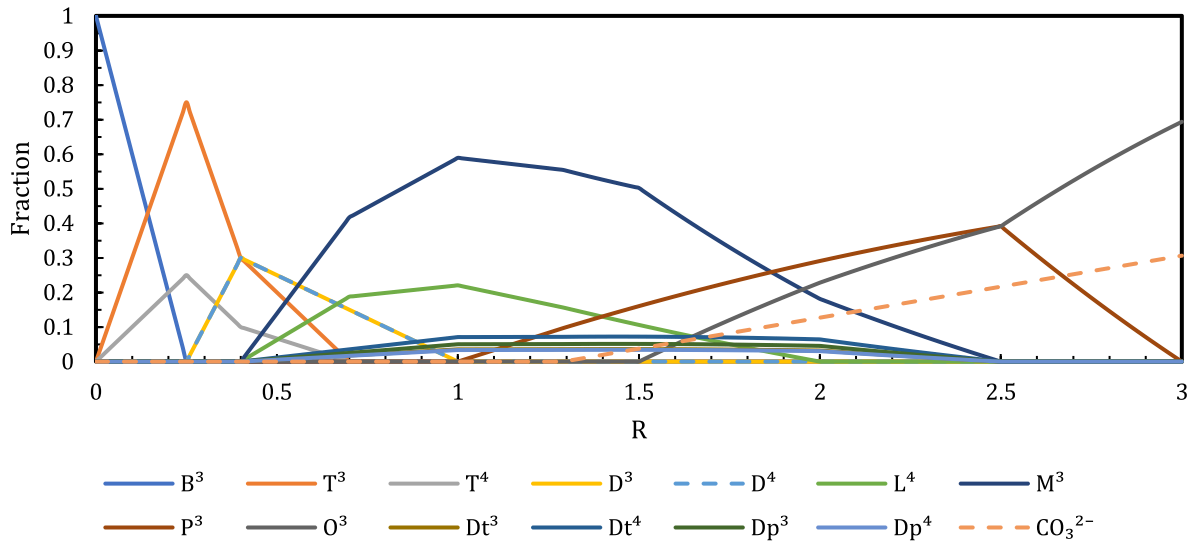

Fig. 4. Intermediate Range Structural model of Sodium Borate Glass ($RNa_2O*B_2O_3$).

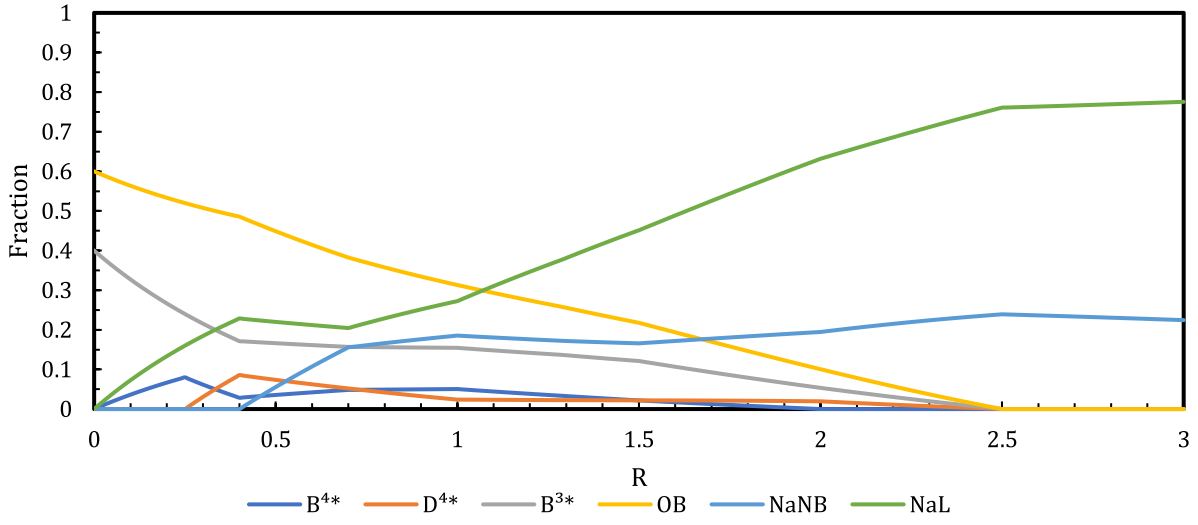

Fig. 5. Fraction of Network Forming Species in Sodium Borate Glass ($RNa_2O * B_2O_3$).

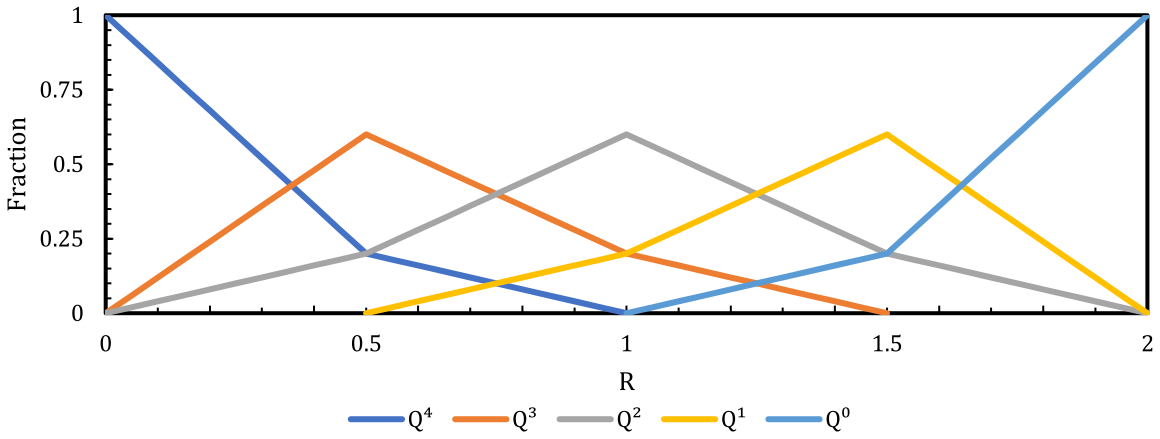

Fig. 6. Structural model of Lithium Silicate Glass ($RLi_2O * SiO_2$).

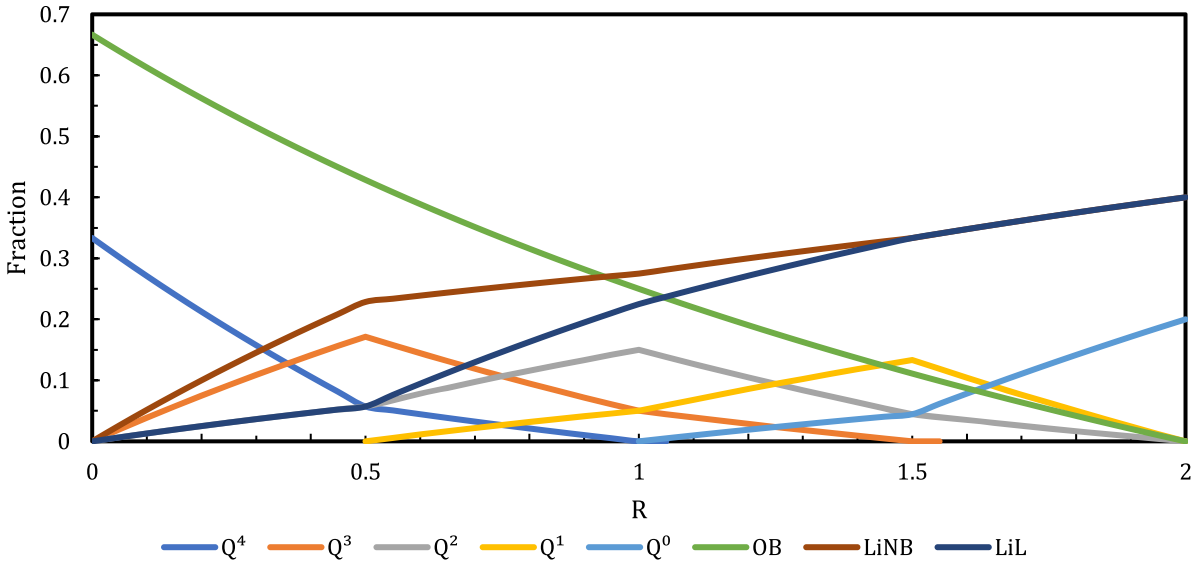

Fig. 7. Network forming species in Lithium Silicate Glass ($RLi_2O * SiO_2$).

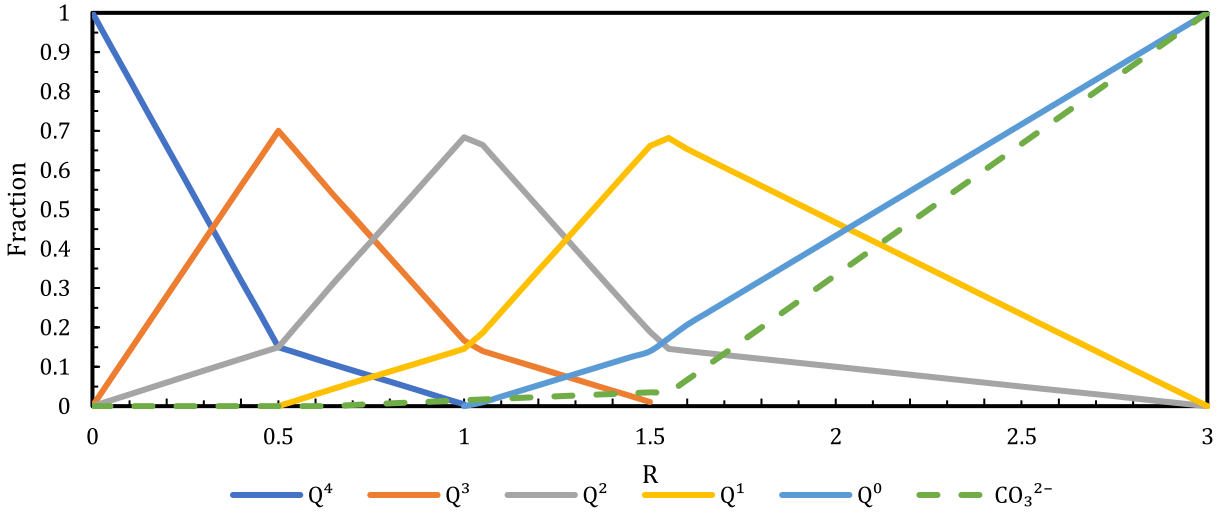

Fig. 8. Structural Model of Sodium Silicate Glass ($RNa_2O * SiO_2$). CO_3^{2-} values are reported as a molar fraction of the total amount of Si in the glass.

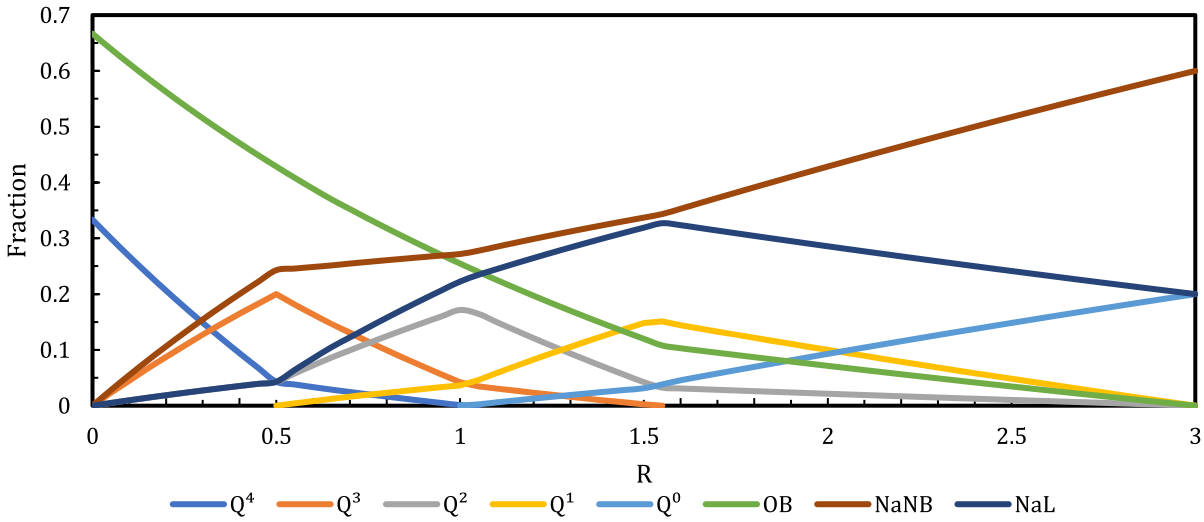

Fig. 9. Network forming species in Sodium Silicate Glass ($RNa_2O * SiO_2$).

considered in oxide glasses [8,10,11]. α-constraints, which are linear, bond-stretching constraints between the glass former atoms and oxygen atoms. β-constraints, which are angular constraints between two oxygens with the glass former atom as the vertex. γ-constraints, which are angular constraints where oxygen is the vertex, either between two network former atoms or a network former and a modifier ion. And finally, μ-constraints, which come from alkali clustering effects. Table 1 shows what each constraint represents, with G being the glass former, such as boron or silicon, O being oxygen, and M* being modifier ions.

A particularly notable property that requires separating these constraints beyond that of linear and angular constraints comes from the temperature dependence of constraints, an advancement in the practice of TCT from Mauro and Gupta [11]. In essence, temperature dependence of constraints is the property of certain constraints to lose their rigidity, or constraining effect, as temperatures increase. This change from rigid to floppy can be modeled as a discrete, binary transition after a certain temperature is reached for the purpose of calculating properties like glass transition. This is important in the case of predicting glass transition temperatures (T_g), as the temperatures at T_g are taken to be higher than that of the γ-constraint's onset temperature. This means that when calculating constraints for use in T_g predictions, γ-constraints are not considered.

This study has also called into place another constraint not accounted for in previous studies on oxide glass system constraints. These constraints are assumed to arise from linear interactions with alkali ions that are not directly associated with a non-bridging oxygen and have been dubbed δ constraints for the purposes of this research.

5. Counting constraints

In relating a structural model to a constraint curve, we need to address all the constraints that come with each structural species. To do this we assign a set type and number of constraints to each structural unit. α-constraints are counted only at the bridging oxygens, with two constraints for each. It should be specifically noted here that non-bridging oxygens are not included for the purposes of α constraints since the linear motion that would typically be restricted by an α constraint would not be of any effect on the network structure overall. β-constraints are counted at the network formers where their vertex lies. The formula $2\langle r\rangle - 3$, where $\langle r\rangle$ is the average coordination of the network former, can be used to find the number of β-constraints associated with each network former. From this we find that each 3-coordinated trigonal planar network forming atom has 3 associated β-constraints and each 4-coordinated tetrahedral network forming atom has 5 associated β-constraints. γ-constraints are counted as one per oxygen, and unlike the α-constraints this does include NBOs, though again for the purposes of calculating T_g these constraints are not considered.

When calculating the two types of alkali constraints, μ and δ, we must split the modifier ions into two different species, 'non-bridging' (M^{NB}) and 'loose' (M^{L}) modifier ions respectively. M^{NB} ions are ions that are directly associated with NBOs in the network structure. The number of M^{NB} ions associated with each structural unit for use in calculating μ-constraints was taken from previous work on constraint models for the lithium and sodium borate systems [8,10]. For each M^{NB} ion there are assumed to be 2 μ-constraints, this number was also taken from previous work [8,10]. The M^{L} ions were assumed to be all modifier ions not associated with μ clustering effects, and 2.5 δ-constraints are assigned to each M^{L} ion. The number 2.5 comes from the linear coordination of alkali ions in the glass, which ^{23}Na NMR data for sodium borate [12], silicate [13], and tellurite [14] glass systems all show to be approximately 5. For systems where carbon is retained in the form of carbonate (CO_3^{2-}) ions, these ions were taken to have no impactful β-constraints and 1 associated M^{NB} ion.

6. Borate constraints

The constraints in a borate glass are relatively simple to calculate from the network forming species shown in Figs. 3 and 5. Using the counting methods described above, we find that each network forming

Table 1
Constraints in Oxide Glasses.

Constraint	Constraint Type
α	linear G-O
β	angular O-G-O
γ	angular G-O-G/G-O-M*
μ	linear O-M*
δ	linear M*-M*

Table 2
Number of Constraints Associated with Network Forming Species.

Species	Number of Constraints	Type of Constraint
B4*	5	β
D4*	4.5	β
B3*	3	β
O^B	2	α
M^{NB}	2	μ
M^{L}	2.5	δ

unit has the number of constraints associated with it shown in Table 2. It is worth reminding that the D4* units (4-coordinated borons in a diborate ring configuration) are counted with an abnormal 4.5 constraints instead of the standard 5 β-constraints for a tetrahedral unit because of the redundantly counted β-constraint inside of the diborate ring shown by Takeda et al. [8]. Plots of the average number of constraints per atom as a function of R for the lithium borate and sodium borate glass systems are shown in Figs. 10 and 11 respectively. For the sodium borate system in Fig. 11 calculations for both glasses with and without retained carbonate are shown.

7. Silicate constraints

The silicate systems' constraints are similarly easy to calculate from the network forming species assembled in Figs. 7 and 9. Since there are no impactful ring structures on constraints or coordination changes in silicate glasses, the only units to consider for constraint counting are the short-range order Q^n units as well as the bridging oxygens and both types of alkali ions. The variation in the average number of constraints is much greater in the alkali silicate glass systems than in their borate counterparts, mainly due to the lack of coordination change and higher amount of NBO's attached to silicate tetrahedra as opposed to borate units, as an increase in NBO's corresponds to a decrease in constraints. Plots of the average number of constraints per atom as a function of R for the lithium silicate and sodium silicate glass systems are shown in Figs. 12 and 13 respectively. For the sodium silicate system in Fig. 13 carbonate effects are included.

8. Glass transition temperature

To calculate glass transition temperature from constraints, we can use the following equation, where R_r is the reference composition, $T_g(R)$ is the glass transition temperature at composition R, and $n[T_g(R),\ R]$ is the number of constraints at composition R [10].

$$T_g(R) = T_g(R_r)\frac{3 - n\left[T_g(R_r), R_r\right]}{3 - n\left[T_g(R), R\right]}\ . \tag{1}$$

Reference compositions R_r are used to align the constraint curves to properties using the constraints and the value of the property at that point. This point is typically chosen to be a well-defined point, where both the structural information and property data is accurately known. In the case of the alkali borate glasses, this point is chosen to be $R_r = 0$, since at this point, the T_g is well defined at around 533 K and the structure is agreed to be made up entirely of 3-coordinated boron units with no NBOs. For the silicate glasses, a reference composition of $R_r = 1$ is chosen. In the silicate case, pure SiO_2 ($R = 0$) is not chosen because pure silicate glass is difficult to produce and its T_g can vary greatly based on imperfections such as the water content of the glass [15]. $R = 1$ is chosen instead as its structural data and properties are more well-defined. For lithium silicate, the reference $T_{g,r} = 721K$, and for sodium silicate, the reference $T_{g,r} = 662K$ [16].

Glass transition temperatures were modeled from constraints using the above methods, and plotted against experimental data. The lithium borate T_g model is shown against experiment [17–19] in Fig. 14. Here we find the TCT model aligns to experimental data strongly both in low and into high alkali ranges. The model applied for sodium borate glass is shown against experiment [17,20–22] in Fig. 15, with a similarly strong agreement reaching far into the high alkali range. Alkali Silicate Glass transition temperature models are shown against experiment [16] in Figs. 16 and 17.

9. Fragility

Another property able to be predicted through TCT is a glass's fragility, though the process is slightly more complex. In order to accurately predict fragility data, a continuous form of temperature dependence must be used in the place of the discrete model used to calculate glass transition temperature. This is because the model relating fragility to constraints involves the derivative of the degrees of freedom with respect to the composition, which is incompatible with the discrete "on/off" model used in calculating the glass transition. Degrees of freedom in this instance are calculated as $f = 3 - n(R)$, where $n(R)$ is the number of constraints at composition R. The equation used model fragility is as follows, where m is the fragility, $f(T,R)$ is the degrees of freedom at a given temperature T and composition R, and m_0 is the fragility of a strong glass, taken to be 14.97 [23].

$$m = m_0\left(1 + \left.\frac{\partial \ln f(T,R)}{\partial \ln T}\right|_{T=T_g(R)}\right). \tag{2}$$

Since we are using the temperature dependent model of constraint theory, calculating the degrees of freedom is not as trivial as in the discrete model, and in this instance the degrees of freedom are measured as the number of each type of constraint multiplied by its temperature dependence coefficient,

$$f(T,R) = \sum 3 - n_c(R)q_c(T), \tag{3}$$

where c represents the different types of constraints, α, β, μ, γ, and δ. In

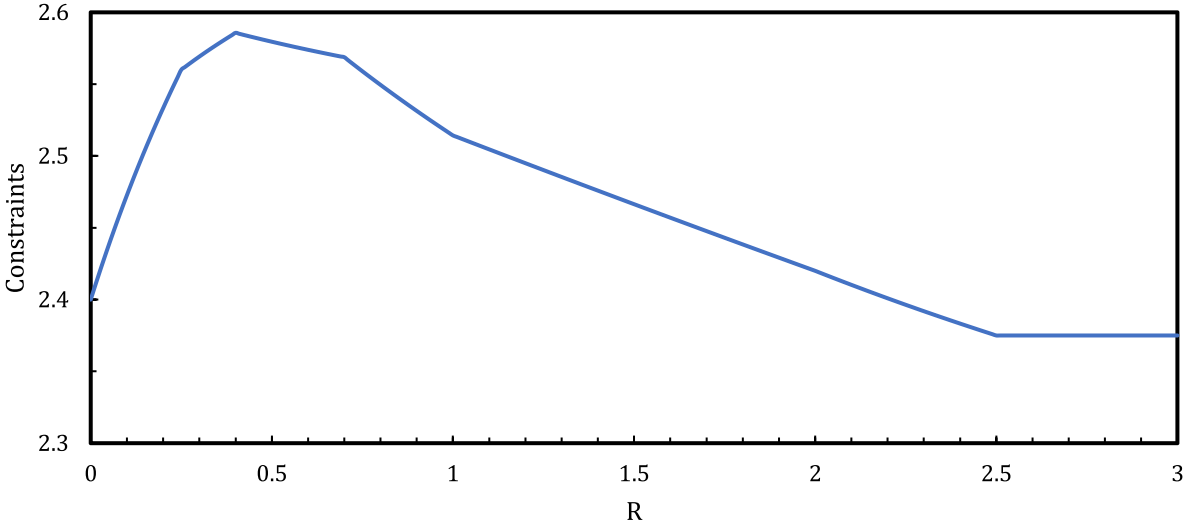

Fig. 10. Average Number of Constraints per Atom in Lithium Borate Glass (RLi_2O * B_2O_3).

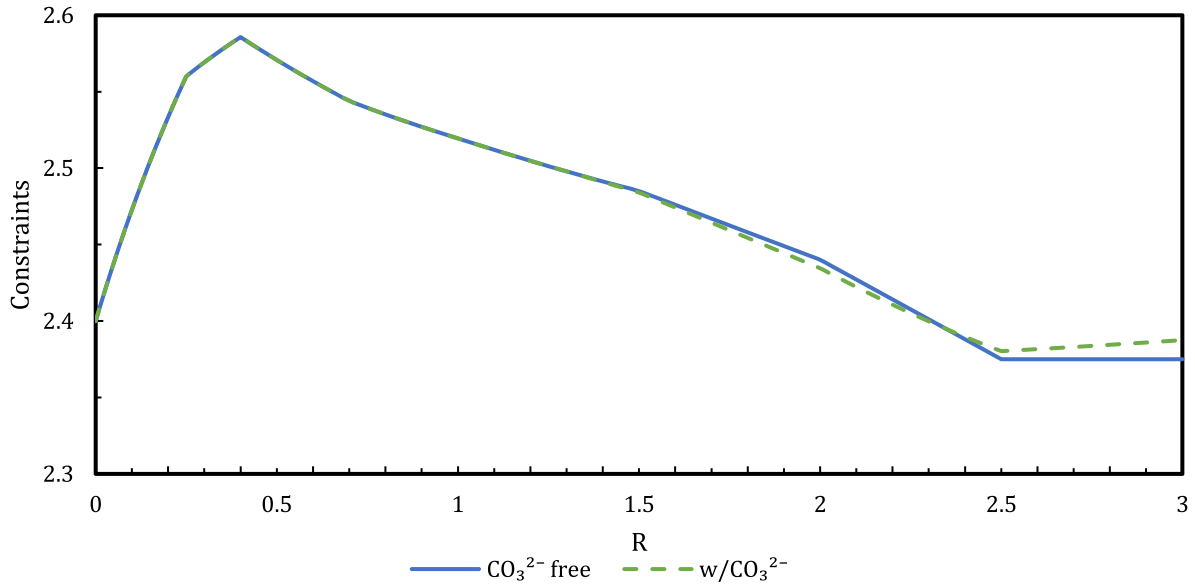

Fig. 11. Average Number of Constraints per Atom in Sodium Borate Glass ($RNa_2O*B_2O_3$).

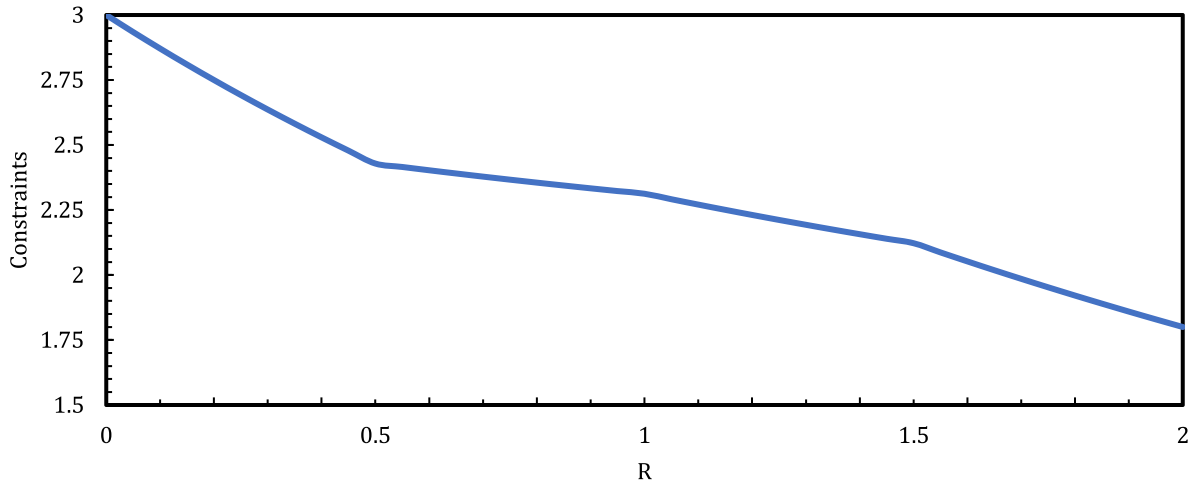

Fig. 12. Average Number of Constraints per Atom in Lithium Silicate Glass ($RLi_2O * SiO_2$).

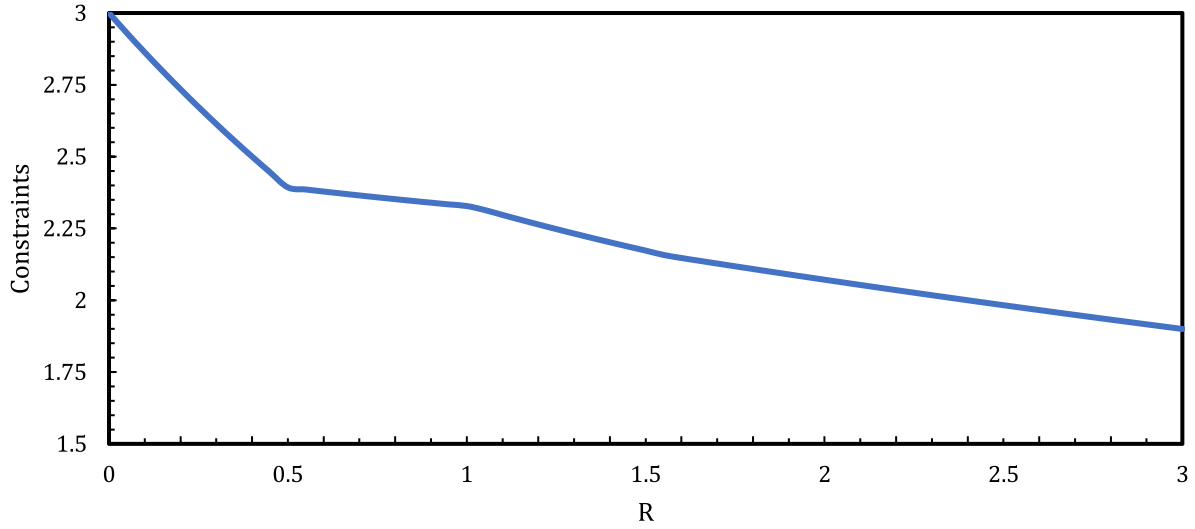

Fig. 13. Average Number of Constraints per Atom in Sodium Silicate Glass ($RNa_2O * SiO_2$).

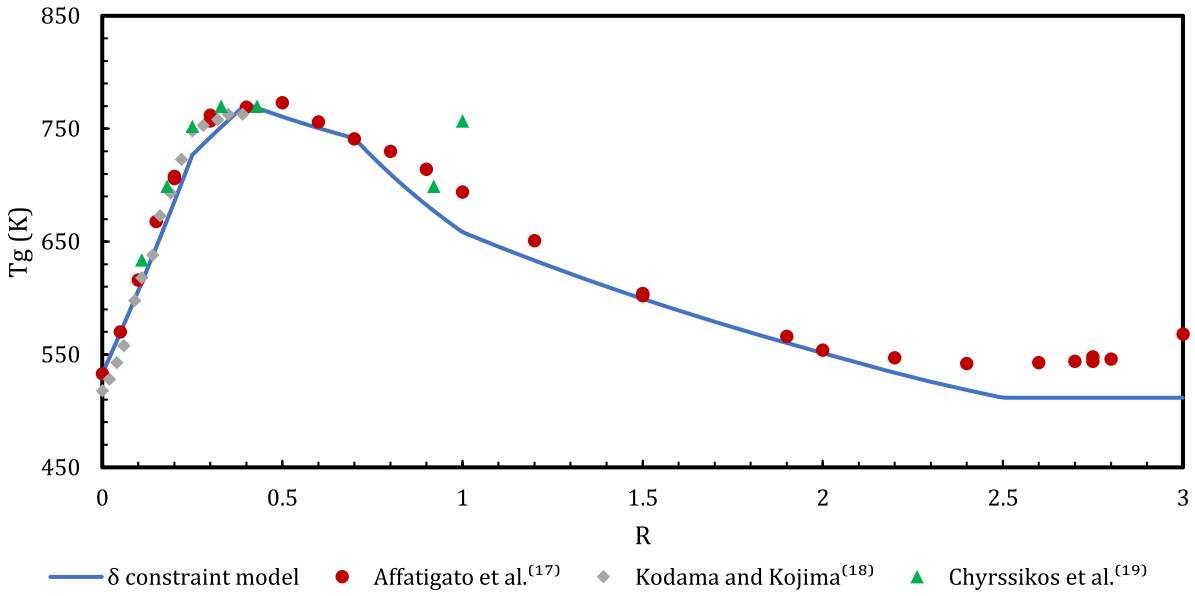

Fig. 14. Glass Transition Temperature for Lithium Borate Glass (RLi2O*B2O3). The error in the data is +/- 4 K. The data markers are larger than the error.

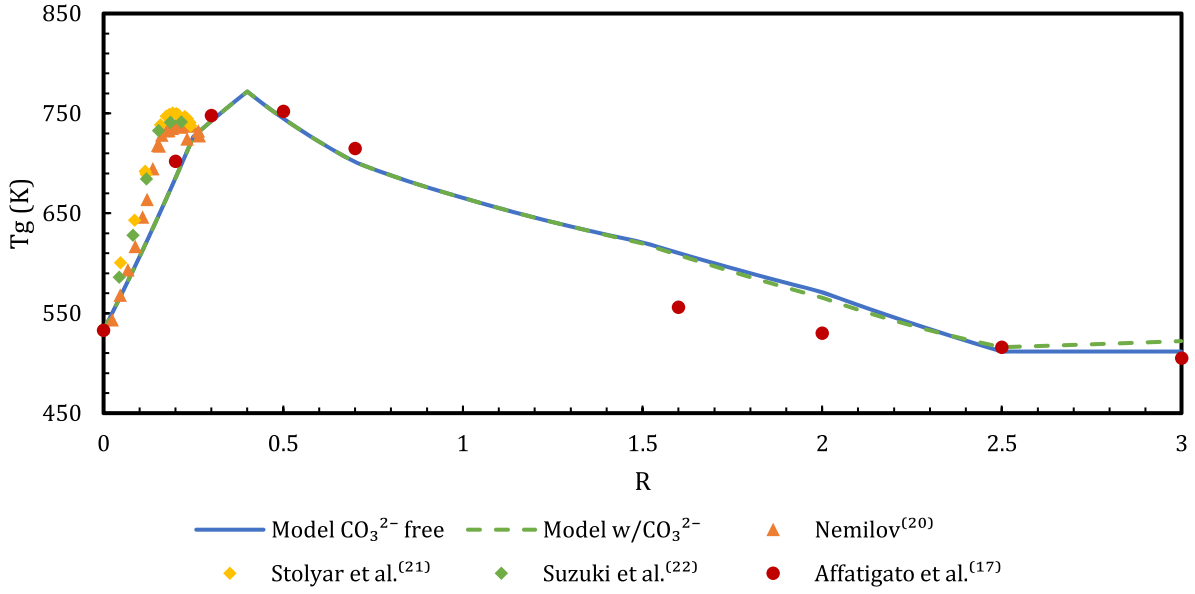

Fig. 15. Glass Transition Temperature for Sodium Borate Glass (RNa2O * B2O3). The error in the data is +/- 4 K. The data markers are larger than the error.

the temperature dependent constraint model proposed by Mauro et al. [24], the temperature dependence coefficient takes the form of Eq. (4).

$$q_c(T) = \left(1 - \exp\left(\frac{\Delta F_c^*}{kt}\right)\right)^{vt}, \tag{4}$$

where vt is the number of escape attempts (a fitting parameter corresponding to the sharpness of the curve, set in this case to 1000 in correspondence with our borate reference point), and ΔF_c^* is the activation free energy for each constraint c. ΔF_c^* is defined by Eq. (5):

$$\Delta F_c^* = -kT_c \ln\left(1 - 2^{\frac{-1}{vt}}\right), \tag{5}$$

where k is Boltzmann's constant and T_c is the onset temperature for each constraint c, where the constraint begins to change from rigid to floppy, and are dependent on both glass composition and constraint type. For borate glasses, constraint onset temperatures were taken to be $T_\alpha = 921K$, $T_\beta = 750K$, $T_\gamma = 328K$, and $T_\mu = 900K$ [24]. The onset temperature of the δ constraints can be roughly estimated within a given range through comparing its physical significance with other constraint onset temperatures. As described by Bødker et al. [25] linear constraints are shown to have higher constraint onset temperatures than their angular counterparts, as corresponding to the strength of the bonds and modes which they represent, taking the order of $T_\gamma < T_\beta < T_\mu < T_\alpha$. Given that we take δ constraints to represent linear modes, it makes sense that $T_\beta < T_\delta$, though given that inter-alkali connections should in theory be weaker than the ionic constraint between a modifier ion and an NBO, it should therefore follow that $T_\delta < T_\mu$. This gives us our range for the constraint onset temperature, which was set at $T_\delta = 850K$. Further work may be necessary to affirm the validity of this value, which as shown by Wilkinson et al. [26] and Potter et al. [15] can be determined through fittings of the Young's modulus and through molecular dynamics simulations.

Results for the lithium borate glass fragility are shown against

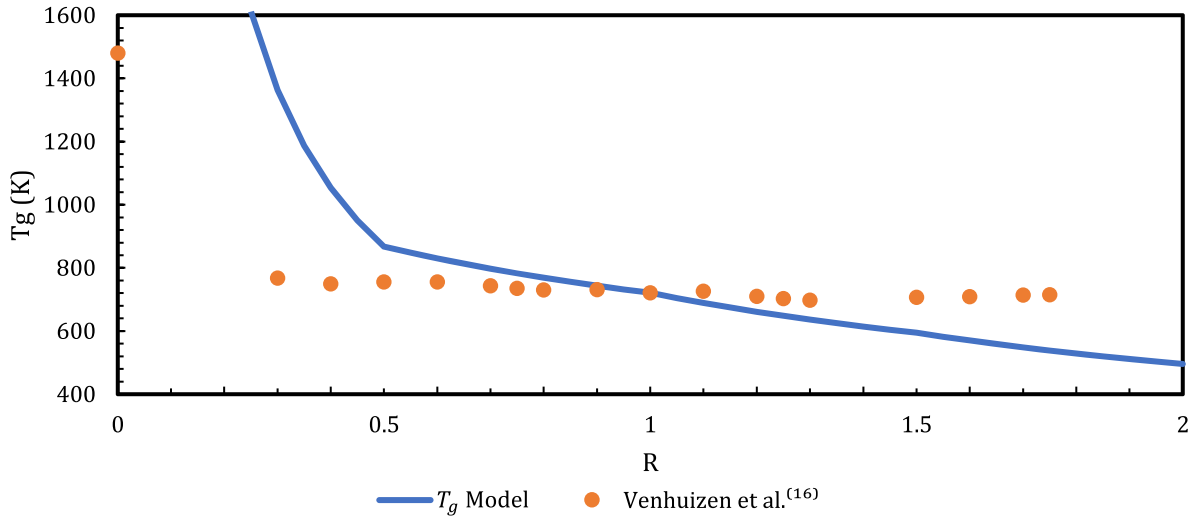

Fig. 16. Glass Transition Temperature for Lithium Silicate Glass (RLi2O*SiO2). The error in the data is +/- 4 K. The data markers are larger than the error.

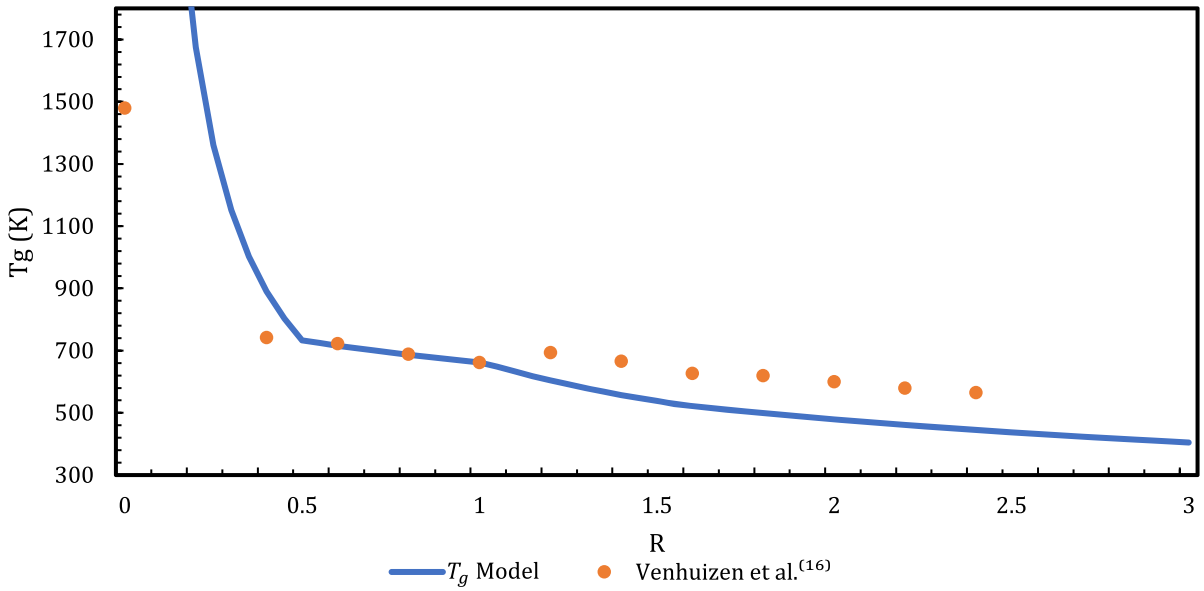

Fig. 17. Glass Transition Temperature for Sodium Silicate Glass (RNa2O*SiO2). The error in the data is +/- 4 K. The data markers are larger than the error.

experimental data [19,27] in Fig. 18. Results for fragility calculations both with and without δ constraints are plotted here to show the added effects it has on the fragility model. Results for the sodium borate system plotted against experimental data [20,21] are shown in Fig. 19. Results for the sodium borate system include δ constraint calculations.

10. δ constraint defense & implication

The successful introduction of a new type of alkali constraint gives some insights into the role of alkali ions in glass structure. These additional constraints were able to greatly improve the accuracy of each system, especially at high alkali ranges, where previous models have begun to falter [8,23], which points to these constraints having some real-world significance. These constraints make use of the ions that are not considered in the clustering effects which are considered for μ-constraints. This split between clustering modifier ions and non-clustering 'loose' ions proposes that some alkali ions are not as directly associated with the glass structure, the number of which appears to be dependent on individual structural units and the localization of their charge. A possible example of the real-world effect that corresponds to δ constraints may come from a metallic interaction between multiple of these loose alkali ions, or also possibly a polar interaction between bridging oxygens and the alkali ions. This idea is supported further by the fact that the number of δ constraints per loose alkali ion that produced the best results was directly related to the average coordination of alkali ions in oxide glasses as shown in ^{23}Na NMR [13].

As shown in Takeda et al. [8], the number of these 'loose' ions can also have some correlation to the conductivity of the glass, though this model is not accurate for all compositions of the glass, namely at high alkali content. Fig. 20 shows a comparison of the model from this work, labelled the "δ constraint model", versus previous constraint theory models for the lithium borate glass system, which shows the significant effect that the δ constraint has, particularly at high R values. The model of Takeda et al. [8] was based, in part, on the work of Smedskjaer et al. [10]. The present model is a refinement of the Smedskjaer model and the result is an improvement in the fit, especially at high R values due to the

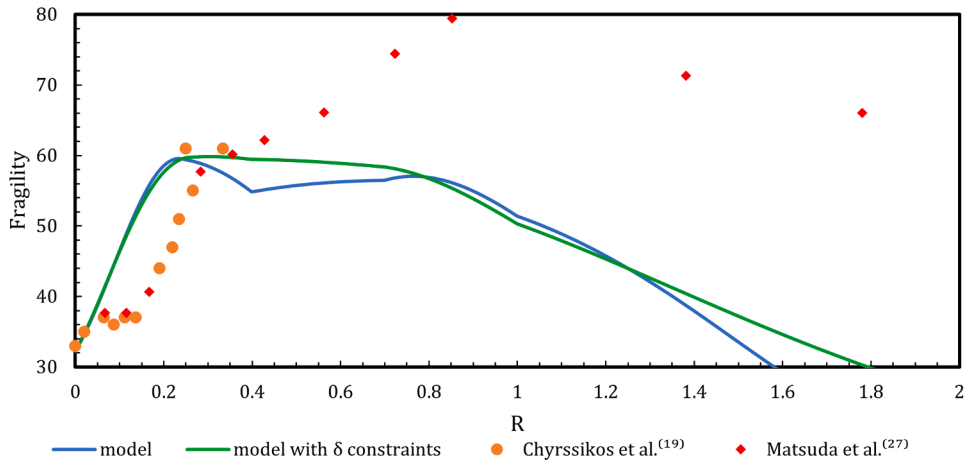

Fig. 18. Fragility for Lithium Borate Glass ($RLi_2O*B_2O_3$).

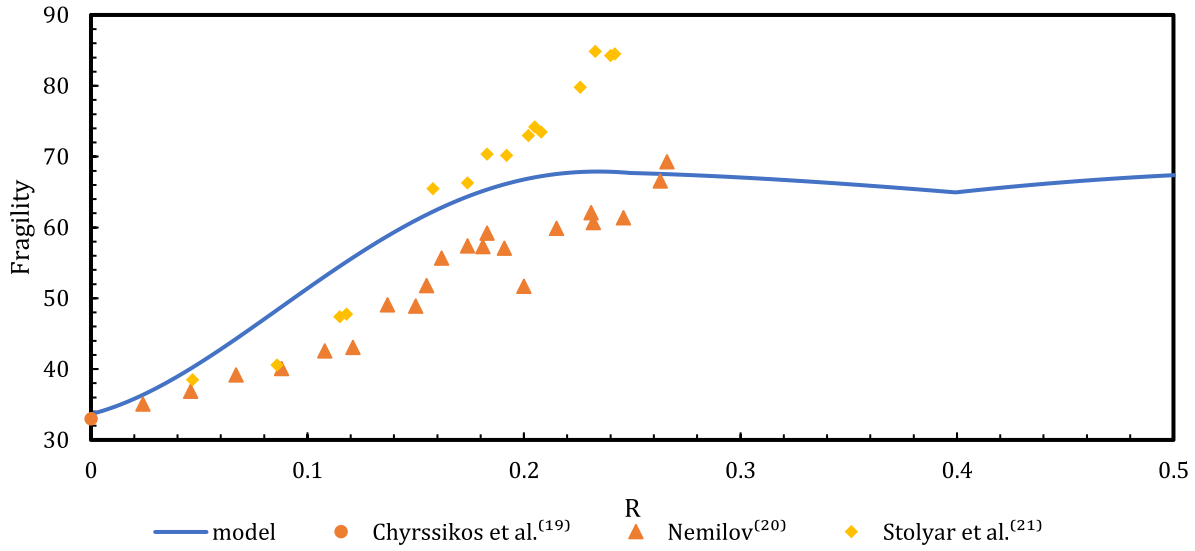

Fig. 19. Fragility for Sodium Borate Glass ($RNa_2O*B_2O_3$).

added δ constraints.

11. Future study & plans

The Methods outlined in this paper should also be applicable to other glass systems, which may also explore the intricacies of how TCT can relate to glass properties. One such system is the alkali borosilicate glasses, which could be used to explore the role and significance of the impact of the reference point and composition used to predict properties when multiple glass forming networks are at play. TCT can also be used to predict properties other than glass transition temperature such as Vickers Hardness, as seen in Fig. 21 which was produced alongside hardness data collected at Coe College by Bragatto [28] for the lithium borate glass system. A noteworthy property of this data is that some of the glasses used were melted in alumina crucibles, which likely led to the contamination of alumina in the glass. This contamination would disrupt the structure and misalign the structural model with the physical structure of the glasses used to find data points. Even still it is a good example of how TCT can be used to predict other properties, as well as an example of TCT's potential shortcomings in real world applications.

12. Conclusions

In both alkali borate glasses studied we see a very strong agreement between the constraint based model and experimental T_g values, however the alkali silicate glasses have significantly worse agreement, particularly in the low-alkali region. In dissecting the reason for the discrepancy between our model and experimental data, we first notice that the average number of constraints per atom for pure SiO_2 glass ($R = 0$), which is made up entirely of tetrahedral Q^4 units will all bridging oxygens, has exactly 3 constraints per atom. Alternatively, it has zero degrees of freedom, and in Eq. (1) which we use to calculate the T_g this results in an infinite asymptote as we approach pure SiO_2. While at first this disagreement may seem irreconcilable, understanding it can both lead to an interesting observation about silicate glass as well as insight into the limitations of TCT. The infinite asymptote for the T_g causes some deviation between model and experiment at low R values. The proposed culprit for the disagreement between model and experiment may primarily come in the form of chemical impurities, specifically water. It has been shown by Potter et al. that in acting as a modifier, small amounts of water can impact the number of constraints seen in silicate glass and bring T_g predictions much more in line with experimental data [15]. The effect a small impurity can have on the predicted value highlights an important limitation of TCT. Since the model relies so heavily on a

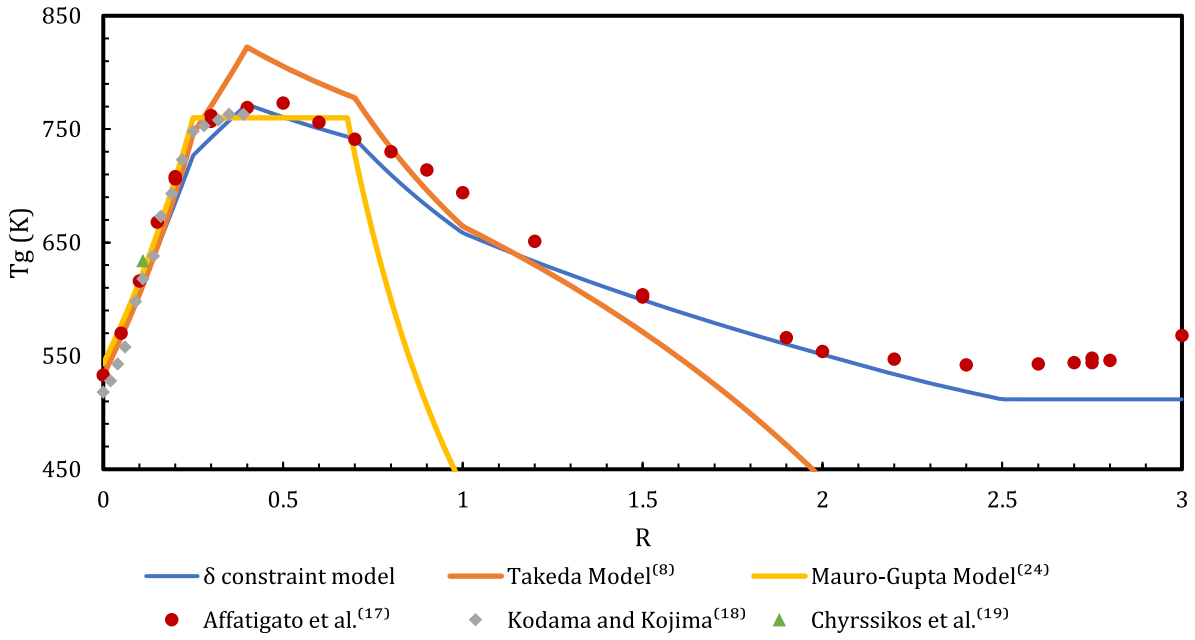

Fig. 20. Comparison of Different TCT Models for Lithium Borate Glass Transition Temperature ($RLi_2O*B_2O_3$).

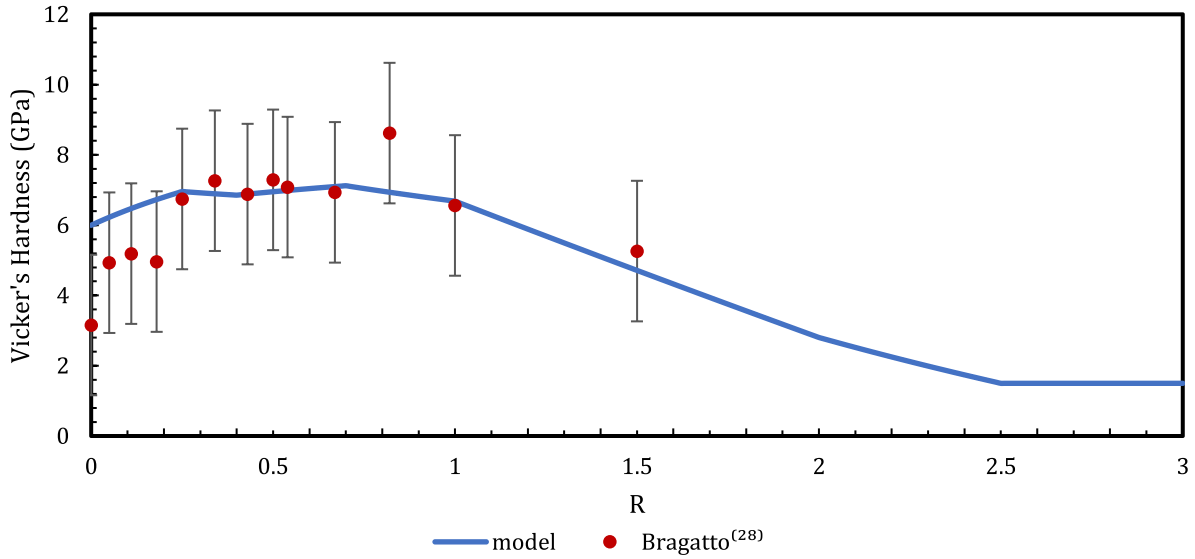

Fig. 21. Vicker's Hardness of Lithium Borate Glass (RLi2O*B2O3). The error in hardness is approximately +/- 2 GPa.

strong understanding of the molecular structure of the glass, any deviation between that structural model and the actual molecular structure of the glass, whether it come in the form of impurities, defects, or a simple misunderstanding of the structure, can have a strong impact on how the model can predict properties. In the case of low-alkali silicate glasses the degrees of freedom is very small, so any change to the constraints can seem disproportionately impactful, though this is still something that should be considered as a source of error in any predictive model using constraint theory. Other constraints affecting the alkali oxides are possible at high R. We believe that this would be a small effect and ignore it here. Another possibility could be a deviation in the amount of non-bridging alkali ions, or in the inter-alkali coordination that arise under saturated conditions seen at high R values. This could potentially impact the behavior of the μ constraints and affect δ constraints, respectively. Inversely, given the strong agreement between model and experiment with the alkali borate glasses, we can assume that there is also likely a very strong agreement between our structural model and the true molecular structure of the glass systems.

While not as strong of an agreement as the glass transition temperature, results for the fragility model are successfully able to recreate the trends shown in experimental data. The notable difference between model and experiment is shown at low alkali, where the model rises significantly faster than the experiment, especially in the lithium borate glass system. At high alkali regions it is also apparent that the model falls significantly below experiment. It is unclear at this time what is causing the inaccuracies in the model. Investigations into parts of the model such as the temperature dependence for each constraint and the role of a fictive temperature could potentially shed light on this discrepancy.

CRediT authorship contribution statement

N. Keninger: Conceptualization, Methodology, Software, Validation, Formal analysis, Investigation, Data curation, Writing – original draft, Writing – review & editing, Visualization. **S. Feller:**

Conceptualization, Methodology, Validation, Resources, Writing – original draft, Writing – review & editing, Supervision, Project administration, Funding acquisition.

Declaration of Competing Interest

The authors declare that they have no known competing financial interests or personal relationships that could have appeared to influence the work reported in this paper.

Data availability

Data will be made available on request.

Acknowledgments

The authors would like to thank the NSF for supporting this research under grant numbers NSF-DMR-1950337 and NSF-DMR-2203142. Dr. Collin Wilkinson is also acknowledged for his insight in direction and troubleshooting, as well as Bryce Reynolds for his help on earlier versions of the models developed through this research.

References

[1] S.A. Feller, W.J. Dell, P.J. Bray, 10B NMR studies of lithium borate glasses, J. Non Cryst. Solids 51 (1) (1982) 21–30, https://doi.org/10.1016/0022-3093(82)90186-7.
[2] G.E. Jellison, P.J. Bray, A structural interpretation of B10 and B11 NMR spectra in sodium borate glasses, J. Non Cryst. Solids 29 (2) (1978) 187–206, https://doi.org/10.1016/0022-3093(78)90113-8.
[3] E.I. Kamitsos, M.A. Karakassides, Structural studies of binary and pseudo binary sodium borate glasses of high sodium content, Phys. Chem. Glas. 30 (1) (1989) 19–26.
[4] J.E. Kasper, S.A. Feller, G.L. Sumcad, New sodium borate glasses, J. Am. Ceram. Soc. 67 (4) (1984) c71–c72, https://doi.org/10.1111/j.1151-2916.1984.tb18833.x.
[5] H. Maekawa, T. Maekawa, K. Kawamura, T. Yokokawa, The structural groups of alkali silicate glasses determined from 29Si MAS-NMR, J. Non Cryst. Solids 127 (1) (1991) 53–64, https://doi.org/10.1016/0022-3093(91)90400-z.
[6] N. Barrow, M. Packard, S. Vaishnav, M.C. Wilding, P.A. Bingham, A.C. Hannon, M. Applier, S. Feller, MAS-NMR studies of carbonate retention in a very wide range of Na_2O-SiO_2 glasses, J. Non Cryst. Solids 534 (2020), 119958, https://doi.org/10.1016/j.jnoncrysol.2020.119958.
[7] J.C. Phillips, M.F. Thorpe, Constraint theory, vector percolation and glass formation, Solid State Commun. 53 (8) (1985) 699–702, https://doi.org/10.1016/0038-1098(85)90381-3.
[8] W. Takeda, C.J. Wilkinson, S.A. Feller, J.C. Mauro, Topological constraint model of high lithium content borate glasses, J. Non Cryst. Solids X 3 (2019), 100028, https://doi.org/10.1016/j.nocx.2019.100028.
[9] C. Larson, J. Doerr, M. Affatigato, S. Feller, D. Holland, M.E. Smith, A 29Si MAS NMR study of silicate glasses with a high lithium content, J. Phys. Condens. Matter 18 (49) (2006) 11323–11331, https://doi.org/10.1088/0953-8984/18/49/023.
[10] M.M. Smedskjaer, J.C. Mauro, S. Sen, Y. Yue, Quantitative design of glassy materials using temperature-dependent constraint theory, Chem. Mater. 22 (18) (2010) 5358–5365.
[11] J.C. Mauro, Topological constraint theory of glass, Am. Ceram. Soc. Bull. 90 (4) (2011) 31.
[12] M. Janssen, 11B{23Na} Rotational echo double resonance NMR: a new approach for studying the spatialcation distribution in sodium borate glasses, Solid State Ion. 136-137 (1–2) (2000) 1007–1014, https://doi.org/10.1016/s0167-2738(00)00535-x.
[13] T. Charpentier, S. Ispas, M. Profeta, F. Mauri, C.J. Pickard, First-principles calculation of 17O, 29SI, and 23Na NMR spectra of sodium silicate crystals and glasses, J. Phys. Chem. B 108 (13) (2004) 4147–4161, https://doi.org/10.1021/jp0367225.
[14] S.L. Tagg, R.E. Youngman, J.W. Zwanziger, The structure of sodium tellurite glasses: sodium cation environments from sodium-23 NMR, J. Phys. Chem. 99 (14) (1995) 5111–5116, https://doi.org/10.1021/j100014a035.
[15] A.R. Potter, C.J. Wilkinson, S.H. Kim, J.C. Mauro, Effect of water on topological constraints in silica glass, Scr. Mater. 160 (2019) 48–52, https://doi.org/10.1016/j.scriptamat.2018.09.041.
[16] P. Venhuizen, A. Peters, R. Williams, S. Feller, A comparison of the densities of lithium and sodium borate silicate glasses with very high alkali contents, in: Proceedings of the Borate Glasses, Crystals, and Melts, Society of Glass Technology, Sheffield, UK, 1997, pp. 498–505.
[17] M. Affatigato, S. Feller, E.J. Khaw, D. Feil, B. Teoh, O. Mathews, The glass transition temperature of lithium and lithium-sodium borate glasses over wide ranges of composition, Phys. Chem. Glas. 31 (1) (1990) 19–24.
[18] M. Kodama, S. Kojima, Anharmonicity and fragility in lithium borate glasses, J. Therm. Anal. Calorim. 69 (2002) 961.
[19] G.D. Chryssikos, J.A. Duffy, J.M. Hutchinson, M.D. Ingram, E.I. Kamitsos, A. J. Pappin, Lithium borate glasses: a quantitative study of strength and fragility, J. Non Cryst. Solids 378 (1994) 172–174.
[20] S.V. Nemilov, A structural investigation of glasses in the B_2O_3–Na_2O system by the viscosimetric method, Neorg. Mater. 2 (1966) 349.
[21] S.V. Stolyar, V.P. Klyuev, A.V. Bulaeva, Viscosity and thermal expansion of Na Borate glasses in the Tg range, Fiz. Khim. Stekla 10 (1984) 447.
[22] S. Suzuki, T. Kobayashi, M. Takahashi, M. Imaoka, Viscosity of some oxide glasses in the glass transition range, J. Ceram. Soc. Jpn. 89 (1981) 252.
[23] P.K. Gupta, J.C. Mauro, Composition dependence of glass transition temperature and fragility. I. A topological model incorporating temperature-dependent constraints, J. Chem. Phys. 130 (9) (2009), 094503, https://doi.org/10.1063/1.3077168. –094503.
[24] J.C. Mauro, P.K. Gupta, R.J. Loucks, Composition dependence of glass transition temperature and fragility. II. A topological model of alkali borate liquids, J. Chem. Phys. 130 (23) (2009), 234503, https://doi.org/10.1063/1.3152432.
[25] M.S. Bødker, J.C. Mauro, R.E. Youngman, M.M. Smedskjaer, Statistical mechanical modeling of borate glass structure and topology: prediction of superstructural units and glass transition temperature, J. Phys. Chem. B 123 (5) (2019) 1206–1213, https://doi.org/10.1021/acs.jpcb.8b11926.
[26] C.J. Wilkinson, Q. Zheng, L. Huang, J.C. Mauro, Topological constraint model for the elasticity of glass-forming systems, J. Non Cryst. Solids X 2 (2019), 100019, https://doi.org/10.1016/j.nocx.2019.100019.
[27] Yu Matsuda, Y. Fukawa, M. Kawashima, S. Mamiya, S. Kojima, Dynamic glass transition and fragility of lithium borate binary glass, Solid State Ion. 179 (2008) 2424–2427, https://doi.org/10.1016/j.ssi.2008.09.011.
[28] C. Bragatto, Unpublished data on hardness of lithium borate glasses, 2021.